Insect visuomotor delay adjustments in group flight support swarm cohesion

Md. Saiful Islam and Imraan A. Faruque

School of Mechanical and Aerospace Engineering
Oklahoma State University, Stillwater, OK, 74078, USA.

*Corresponding author(s). E-mail(s): saiful.islam@okstate.edu;
Contributing authors: i.faruque@okstate.edu;

Abstract

Flying insects routinely demonstrate coordinated flight in crowded assemblies despite strict communication and processing constraints. This study experimentally records multiple flying insects tracking a moving visual stimulus. System identification techniques are used to identify the tracking dynamics, including a visuomotor delay. The population delay distributions are quantified for solo and group behaviors. An interconnected visual swarm model incorporating heterogeneous delays is developed, and bifurcation analysis and swarm simulation are applied to assess swarm stability under the delays. The experiment recorded 425 insect trajectories and quantified visual tracking delay variation. Solitary tasks showed a 30ms average delay and standard deviation of 50ms, while group behaviors show a 15ms average and 8ms standard deviation. Analysis and simulation indicate that the delay adjustments in a group act to improve swarm formation and center stability. These results quantify the role of visuomotor delay heterogeneity in flying insects and their role in supporting swarm cohesion.

Keywords: Tracking system, system identification, system delay, swarm model, attraction potential, mean field analysis, heterogeneous delays

1 Introduction

A significant barrier to creating adaptive swarms of small scale unmanned aerial systems and other challenging robotic swarms remains the provision of fast, computationally-lightweight sensing and feedback structures to support relative navigation in dynamic groups [1–3]. Insects flying in groups can serve as model systems for resource-constrained feedback on these swarming micro air vehicles [4]. Despite tight constraints on sensory and neural feedback mechanisms and the lack of a conventional communication network, insects in naturalistic swarms coordinate flying movements in close proximity to dynamically changing numbers of neighbors in unstructured environments. Visual control may be a critical tool for implicit communication, given the large fraction of insect neural resources dedicated to visual processing. Vision is one of the few insect sensor modalities with quantifiable bandwidth, range, and sensitivity that could provide real-time data to adjust trajectories [5, 6], yet the specific processes supporting inflight feedback in insect group behaviors remain unknown. Many theoretical swarm models and numerical studies have not yet been integrated with experimental investigations on naturalistic swarms, limiting the ability of theory and experiment to inform each other.

A critical need is understanding the way in which these animals manage individual sensing and feedback processing delays, which may be changing or show population-wide diversity. Many animals (and aerial robotic implementations) show a nonzero latency or reaction delay due to sensory processing. The effect of individual agent heterogeneity in latencies in swarming experiments has not been adequately related to theoretical findings, with experimental studies reporting average delays rather than quantifying the distributions of individual delays. We previously quantified the visuomotor delay seen in flying insects tracking a moving visual stimulus in a solitary task [7]. To isolate how these sensory processing delays may be modified in group flight, a new experimental tool is designed that can record visual tracking trajectories in both solo and group tasks.

A moving stimulus (hive entrance) is oscillated horizontally while honeybees fly through it. The dynamic model is then explored using a system identification approach employing these tracking trajectories, isolating the change in dynamic structure for solitary and group bees. The experimental results indicate that the insects have heterogeneous processing delays, and both the heterogeneity and magnitude of the delay are reduced in group tasks, with two different gamma distributions fitting the data. These findings inform the development of a visually-guided swarm model incorporating heterogeneous delays. The visual swarming model integrates the measured delay distributions to predict regions of stable and unstable swarm behaviors, and a simulation of the modeling framework verifies that the swarm behavior stability results persist with experimental delays and for configuration stability.

The remainder of this paper is structured as follows. Section 2 reviews previous works on insect tracking experiments and their application on swarm network. Section 3.1 describes the experimental tool based on a flight arena equipped with a moving stimulus and a real-time insect tracking routine called Visual Input System Identification from Outputs of Naturalistic Swarms (VISIONS) in Section 3.2, and uses these tools to experimentally identify the visual processing and feedback delay across different insects freely flying in insect behaviors. The identified delays are measured at the individual insect level, and methods to quantify experimental probability distributions are described in Section 3.4. In Section 4, the swarm level effect of heterogeneous delay distributions and their connection to theoretical swarm modeling are developed through mean field and bifurcation analysis to determine how measured changes in the distribution's probability density function affect swarm behavior (stability and cohesion). Section 5 explores the outcomes of the experiment, theory, and simulation results, while Section 6 summarizes the study and conclusions.

2 Related work

Previous foundational results in this area have primarily leveraged either experimental or theoretical paths.

Experimental

Animals serve as model systems for collective behaviors serving a group interest, such as migration, foraging, and predatory sensing and defence. Group behavior implies that complicated interactions may be used to make decisions among themselves [8–10]. Direct application of stimuli to swarm can result in deviations from their usual biological to adaptive behaviors [11–13]. The effects of environmental stimuli examining insect flight behavior and motions during visually-dominated behaviors like obstacle avoidance, landing on a wall or proboscis, and flower tracking have previously focused most on the role of ambient and external illumination levels [14–16]. Insect flight trajectories can be tracked and recorded through several existing software tools [17–21]. For studies involving precise timing of an insect or collection of insects tracking a visual stimulus, the recording of visual stimulus in the background is also necessary for accurate analysis. Midge swarms regulate themselves relative to a dynamic moving stimulus which reveals possible interactions present in their common activity [22]. Swarm markers and light intensity experiments with *Chironomus riparius* in a laboratory environment indicated that pheromones can be a important role in swarm cohesion, and these midge swarms suggest that relatively small numbers of agents (e.g., 10 agents) are sufficient to saturate statistical measures of swarm behavior [23, 24]. Flower tracking investigations on *Manduca sexta*

hawkmoths using a moving flower at various frequencies indicate tracking performance during feeding and energy expenditure, revealing that flower movement direction has a stronger effect on tracking performance than the target's movement frequency [25]. When flying in wind, the unsteady flight of a hawkmoth in the wake of a 3D printed robotic flower displays larger tracking overshoot and a reduced order dynamic system [26] and a flower tracking experiment was used to quantify the change in their flight behavior under various light conditions, with average flower tracking behavior represented by a simple temporal delay at various light intensities [27]. By adjusting light intensity, a system identification approach was utilized to find a brightness-dependent delay term in the transfer function, resulting in a dynamic model for each Hawkmoth variant that included a combination of species-dependent scaling parameters and processing delays [28]. There is evidence to suggest the delay associated with a swarm's motion may have a dependency on number of agents in mosquitoes tracking a moving marker [29]. Neuronal networks with delays in biological examples can have a significant role on observed biological behaviors, including generating oscillatory motions and periodic signals [30–32]. Despite the rich history of experimental study, measurements of how processing delays are distributed among swarming individuals are not yet available.

Theoretical

Mathematical descriptions of collective motions of multi-agent biological systems, including bacterial colonies, slime molds, locusts, and fish, have become available in the last few decades [33–35]. These models range from continuous approximations and kinetic theory structures to models at the individual level [36–39], with interaction mechanisms often consisting of attractive and repulsive forces [40, 41] affecting particle motion. Swarm characteristics such as cohesion, velocity alignment, and predator avoidance can be achieved in swarms of dynamic models via bifurcation parameters located in the attractive and repulsive potentials [42–44]. An individual agent's influence on swarms is posed using zone based models and communication topological analysis indicates that the attraction and alignment weights affects the group behavior and structure [45]. The swarm's collective behavior can also be described by elastic or thermodynamic analogies where external stimulus can represent the midge swarm behavior [46]. Despite the availability of rigorous proofs for sufficiency of velocity alignment (e.g. [47]), theoretical models have often relied on a high level of instantaneous connectivity that may be impractical in nature or robotic implementations. While experimental research is beginning to understand the need to quantify internal delays due to insect sensing and feedback, these previous studies are limited to reporting a single average delay across all animals and do not yet account for the heterogeneity of delays across the population or the effect of such delays on neighbor-coordinated behaviors. Delay differential equations (DDE) have been used to explore biological delay models with homogenous delays or delays belonging to discrete or continuous distributions [48–51]. Recently, rigorous mathematical analysis and role of delays such as auto regulations, feedback loops, etc. in biological models have been used to describe the quantitative and qualitative behavior of such systems analytically [52]. Lyapunov analysis has recently been used for time delays on swarms composed of first and second order systems to find conditions for swarm stability under homogeneous delays [53]. The theoretical effects of delay in such a network of interaction rules has previously been investigated primarily numerically by distributing delays among agents and applying a mean field analysis [54, 55]. The delays across the agents were modeled as heterogeneous, drawn from a Gaussian distribution.

Role of this study

Theoretical work on delay modeling and experimental work on delay quantification have largely remained distinct, and there is a need to understand how measured delays affect swarm behavior. The main contribution of this paper is to use experimental and theoretical tools to investigate the influence of visual delays on insect swarm behavior. This study connects these areas to address several questions: (a) what is the population-wide distribution of insect inflight processing delays, (b) does this distribution change in solo vs group behaviors, and (c) if so, how does it affect visually-guided multi-agent (e.g., group and swarming) behaviors?

3 Methods

Figure. 1a depicts the overall study, including experimental work, theoretical analysis, and simulations. The measurement system consists of three cameras with angular separations from 50 to 90 degrees as seen in Fig. 1b. Honeybees were recorded entering and exiting a hive entrance actuated to move horizontally as in Fig. 1d. Insects were recorded while approaching the entrance in both solitary and multi-agent conditions. The experimental equipment consists of a moving entrance stimulus design and an imaging system.

3.1 Stimulus design

The entrance stimulus was a 2-inch square hole (tunnel entrance) that could be moved horizontally left and right using triangular frequencies along the world frame's X axis. This setup included two stepper motors (Nema 23) and a motor driver (a4988), which was controlled by a micro-controller (Arduino Uno). The entire circuit diagram is depicted in Fig. 1c which directs the motors according to triangular frequencies.

3.2 Imaging system

The VISIONS [7] tracking system was used to record insect trajectories during solitary and group flight conditions. This study updates the tracker to track multiple insects. The functions in the tracking system are shown in Fig. 2a. To expand tracking from prior single agent tracking with VISIONS to multiple insects, we incorporated data association to match corresponding positions of each camera. The functions in the association algorithm are shown in Fig. 2b.

The intrinsic and extrinsic parameters of the cameras were calibrated via bundle adjustment [56]. For each insect, we calculate reconstructed 3D points from all possible combinations of 2D points and then reproject them from 3D to 2D. We use the intended match from this error list if the re-projection error (difference between observed and re-projected 2d points) is less than the desired accuracy. A set of m insects' 2D positions of camera-1 at time t is described as $H_{1,t} = \{h_1^1(t), h_1^2(t), h_1^3(t), ...h_1^m(t)\}$. Between camera-2 and camera-N_c, the possible combinations for each insect in $H_{1,t}$ is $c = m^{N_c-1}$. The re-projected 2D points vector is $D_j = \{d_1, d_2, d_3, ..., d_j\}$, when $j = 1...c$. The associated agent is taken to be

$$\text{associate}\,(h_1^m(t)) = \min_{j=1,2....c} \|h_1^m(t) - D_{1..j}\| < \sigma \ , \tag{1}$$

where σ is the desired accuracy.

3.3 Data segmentation

We segmented insect's trajectories while they approached and entered the moving entrance. Insect trajectories were assigned a label of solo or group behavior based on the number of agents detected and on the coherence of each insect when multiple insects were measured, as defined in Section 3.4 and illustrated later in Fig. 8c.

3.4 System identification

We identify systems in both the time and frequency domains between the movement stimulus and the insect position. Frequency domain identification is accomplished when record lengths are sufficient (>1.5sec) and time domain when records are shorter.

3.4.1 Frequency domain identification

When the trajectory had sufficient frequency content (trial length), we applied the identification approach for the transfer function $G(s)$ of the insect's position response to stimulus motion via Chirp Z transform (CZT) developed in our prior work [7] and illustrated in Fig. 3. In the frequency domain, frequency response of target tracking is described by gain, phase, and coherence. Coherence $\gamma^2(s)$ is calculated from the spectral and cross-spectral densities of input and output signals as

$$\gamma^2(s) = \frac{\|S_{xy}(s)\|^2}{S_x(s)S_y(s)} \ , \tag{2}$$

where $S_{xy}(s)$ denotes the cross spectral power density and $S_x(s)$ and $S_y(s)$ represent the auto power spectral density of the stimulus (input) and bee (output) coordinates, respectively. The coherence between the stimulus and insect trajectories was used to determine the linear connection throughout the frequency range. We use the frequency response function $G(s)$ obtained from CZT transform by reference to a transfer function with an internal delay time τ to examine the flight dynamics and visuomotor delay of the tracking behavior.

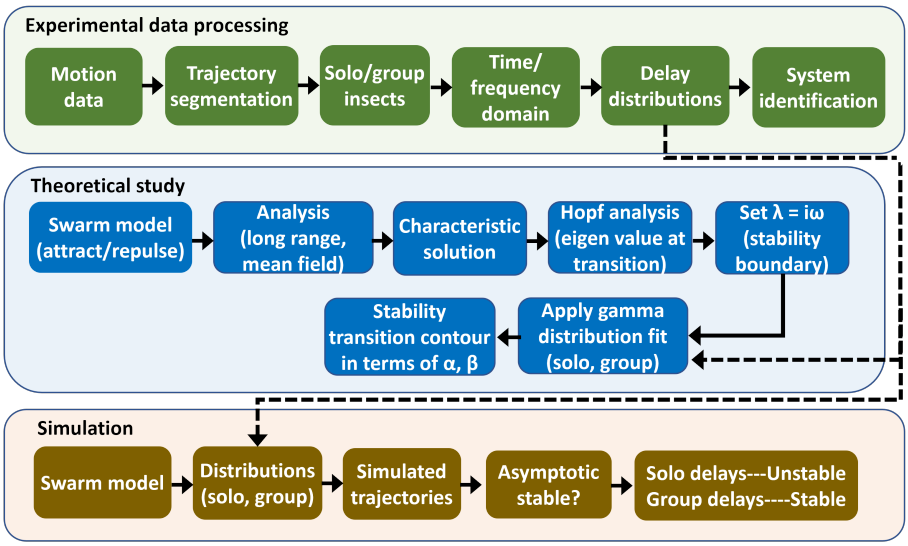

(a) Overall study: experiment, theory, and simulation

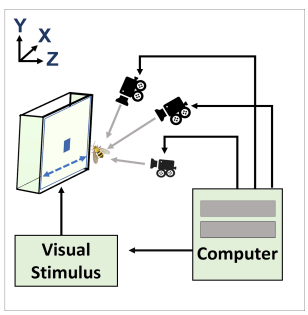

(b) Experimental concept

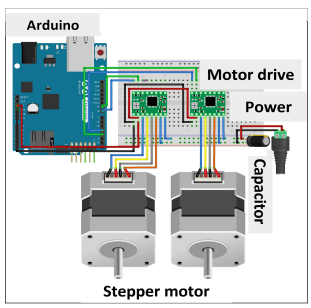

(c) Stimulus mechanism

(d) Experimental setup

Fig. 1: The overall study (a) incorporates three components: a multi agent tracking experiment, theoretical analysis, and simulated performance. A three camera-based tracking system (b) was used to record flight paths of multiple insects (and stimulus) tracking a moving hive entrance actuated by an Arduino micro-controller and stepper motors (c), mounted in an outdoor environment (d).

We conduct the system identification technique across several possible estimated transfer functions $G_e(s)$ and varying time delays $\tau_i \in [0, 200]$ ms. The identified transfer function minimizes the absolute difference between measured frequency response and estimated transfer functions over the region of coherence as

$$\min_{\tau_i, G_e} \|G(s)e^{-s\tau} - G_e(s)e^{-s\tau_i}\|_{s=j\omega,\ \text{s.t. } \gamma^2(s)>0.7.} \tag{3}$$

Three fit criteria FIT, MSE (mean square error) and FPE (final prediction error) are used to determine the best dynamics model [7].

3.4.2 Time domain identification

For the time domain system identification, normalized least square estimation is used to find the dynamic system [57]. The discrete time domain representation of the stimulus and insect are $x_1(k)$ and $x_2(k)$, and by considering a unknown transfer function it can be written as

$$\frac{x_2(z)}{x_1(z)} = \frac{b_1 z^{-1} + b_2 z^{-2} + ...b_n z^{-n}}{1 + a_1 z^{-1} + ... + a_n z^{-n}}, \tag{4}$$

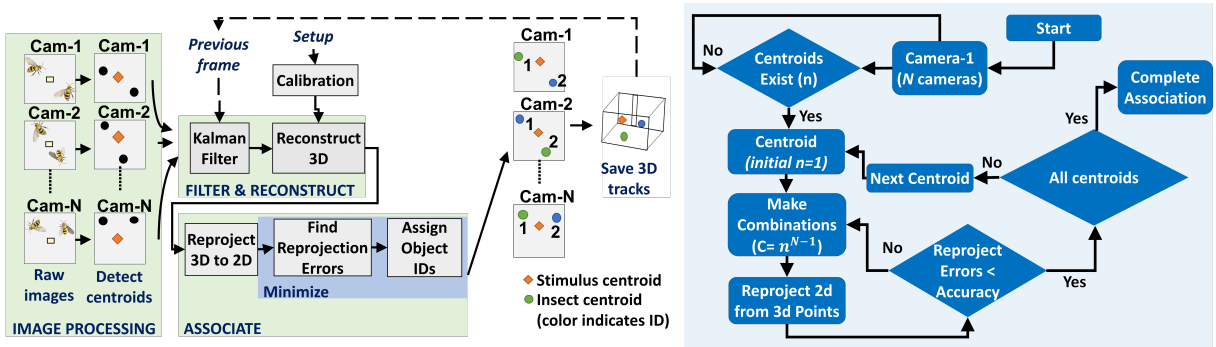

(a) Tracking system (b) Association algorithm

Fig. 2: Flowchart of tracking and association algorithms for VISIONS multi-agent tracker.

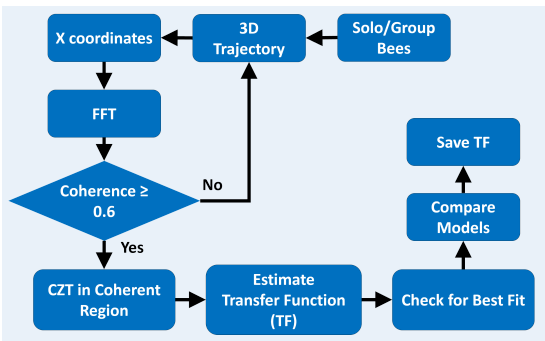

Fig. 3: Frequency-domain system identification flowchart.

where the unknown coefficients are $a_i, b_i;\ i = 1...n$. The time domain solution can be written as

$$x_2(k) = -a_1 x_2(k-1) .... - a_n x_2(k-n) \\ +b_1 x_1(k-1) + ... + b_n x_1(k-n). \tag{5}$$

Then we construct a parametric model, $x_2(k) = \phi^T(k)\theta^*$ where

$$\theta^* = [a_1\ a_2\ .....\ a_n \quad b_1\ b_2 .....\ b_n]^T, \tag{6}$$

$$\phi(k) = [-x_2(k-1)\ ....\ -x_2(k-n) \\ x_1(k-1)\ ....\ x_1(k-n)]^T. \tag{7}$$

The cost function is written as

$$J = \sum_{k=0}^{M-1} (x_2(k) - \phi(k)^T\theta), \tag{8}$$

where $k = 0....M$. The solution $\hat{\theta} = \text{argmin}_\theta\, J(\theta)$ is

$$\hat{\theta} = \sum_{k=0}^{M-1} (\phi(k)\phi(k)^T)^{-1} \sum_{k=0}^{M-1} \phi(k) x_2(k). \tag{9}$$

The fit criterion is defined as

$$f = 100 \times \frac{\|x_2 - \hat{x_2}\|}{\|x_2 - \text{mean}(\text{x}_2)\|} \tag{10}$$

where $\hat{x_2}$ is the predicted output.

4 Swarm model

We can construct a model ofa visually interconnected swarm with agents experiencing visual processing delays by applying a first order dynamic system model with N number of agents and postulating that the agents experience delayed interconnections with each. We build upon previous models with constant delays [53] to develop a swarm model with heterogeneous delays and weighting factors. The swarm model is

$$\frac{dx_i}{dt}(t) = -\nabla_i A^a(x_{ij}, \tau_{ij}) - \nabla_i A^r(x_{ij}, B_r, D_r)\,, \tag{11}$$

where x_i is (vector) position of the agent i, $\nabla_i A^a(x_{ij}, \tau_{ij})$ and $\nabla_i A^r(x_{ij}, B_r, D_r)$ are attractive and repulsive potentials respectively, specified

as

$$A^a(x_{ij},\tau_{ij}) = \frac{1}{2}\left(\sum_{i=1,i\neq j}^{N}(\alpha x_i(t) - \beta x_j(t-\tau_{ij}))\right)^2 \tag{12}$$

and

$$A^r(x_{ij},B_r,D_r) = \sum_{i=1,i\neq j}^{N} B_r e^{\frac{-1}{D_r}|\alpha x_i(t)-\beta x_j(t-\tau_{ij})|}. \tag{13}$$

Here, τ_{ij} is the delay from agent i to agent j, α is the egocentric influence weight and β is the neighbor influence weight. B_r and D_r are the amplitude and applied distance of repulsive potential. At long range, stability may be determined by only the attractive potential and conversely at short range, stability may be determined by considering only the repulsive potential [7, 44]. So, for the mean field analysis we consider only the attraction potential. The center of mass of the swarm can be defined as a vector $C(t)$ as

$$C(t) = \frac{1}{N}\sum_{i=1}^{N} x_i(t)\,. \tag{14}$$

To find the position stability of the swarm, the norm of swarm center is found as $\|C(t)\| = \sqrt{C_x^2(t)+C_y^2(t)}$, where C_x, C_y are the X and Y coordinates of the swarm center respectively. Swarm center stability is then $\|C\| \to$ constant as time $t \to \infty$.

4.1 Mean field analysis

Each agent is updated as

$$\dot{x_i}(t) = -\frac{1}{N}\sum_{j=1,i\neq j}^{N}(\alpha x_i(t) - \beta x_j(t-\tau_{ij})). \tag{15}$$

The position of each agent $x_i(t) = C(t) + \delta x_i(t)$ and δx_i is the deviation from the center of mass C. The position derivative $\dot{x_i}$ is written as

$$\begin{aligned}\dot{x_i}(t) &= \dot{C}(t) + \delta\dot{x_i}(t)\\ &= -\frac{\alpha(N-1)}{N}[C(t)+\delta x_i(t)]\\ &\quad + \frac{\beta}{N}\sum_{j=1}^{N} C(t-\tau_{ij}) + \delta x_j(t-\tau_{ij})].\end{aligned} \tag{16}$$

Summing over i and taking $\sum_i^N \delta x_i(t) = 0$,

$$\begin{aligned}\dot{C}(t) &= -\frac{\alpha(N-1)}{N}[C(t)+\delta x_i(t)]\\ &\quad + \frac{\beta}{N^2}\sum_{i=1}^{N}\sum_{j=1}^{N} C(t-\tau_{ij}) + \delta x_j(t-\tau_{ij})].\end{aligned} \tag{17}$$

We can obtain the center of mass by approximation considering a double sum [54]. The discrete terms can be approximated by a distributed density function $g_\tau(\tau)$. We can extend the discrete delays towards a distributed density function such as

$$\begin{aligned}&\frac{\beta}{N^2}\sum_{i}^{N}\sum_{j}^{N}\delta x_j(t-\tau_{ij})\\ &= \frac{\beta}{N^2}(N-1)\int_0^\infty \sum_{j}^{N}\delta x_i(t-\tau)g_\tau(\tau)d\tau = 0,\end{aligned} \tag{18}$$

with the same approximation made for the center of mass $C(t)$. For large number of agents $\frac{N-1}{N} \approx 1$. Finally, we can write the swarm center dynamics as

$$\dot{C}(t) = -\alpha C(t) + \beta\int_0^\infty C(t-\tau)g_\tau d\tau, \tag{19}$$

which is now a general differential equation in the form

$$\frac{d(C(t))}{dt} = F(C(t),\bar{C}(t)), \tag{20}$$

where $\bar{C}(t)$ is a delay weighted state given by

$$\bar{C}(t) = \int_{\tau_m}^{\infty} C(t-\tau)g_\tau d\tau \equiv \int_{-\infty}^{t-\tau_m} C(t)g_\tau(t-\tau)d\tau. \tag{21}$$

Here, τ_m is the minimal delay and g_τ is the probability density function of the distribution, such that $\int_0^\infty g_\tau d\tau = 1$.

4.2 Hopf bifurcation

We want to examine the sensitivity of the swarm's local stability to changes in distribution shape. The gamma distribution has a relation between its mean with the shape. To examine local stability we need to linearize the system at a steady state solution. By taking $C(t) = ce^{\lambda t}$ in Eqn. (20) we obtain the characteristic solution

$$\nabla\lambda = \lambda + \alpha - \beta \int_0^\infty e^{-\lambda\tau_m} g_\tau(\tau) d\tau = 0. \quad (22)$$

We want to examine how delay affects stability, and apply the fact that the stable/unstable transition takes place when the characteristic equation has a root with zero real part. The density of the gamma distribution is

$$g_\tau(\tau) = \begin{cases} 0, & 0 \le \tau < \tau_m \\ \frac{a^m}{(m-1)!}(\tau - \tau_m)^{m-1} e^{-a(\tau-\tau_m)}, & \tau_m \le \tau \end{cases}. \quad (23)$$

The unshifted density of the distribution can be written as $E = \int_0^\infty \tau g_\tau d\tau = \frac{m}{a}$, where parameters (a, m) specify the shape of the gamma distribution. The gamma distribution's variance is $V = \frac{m}{a^2}$, and its Laplace transform is

$$G_\tau(\lambda) := \int_0^\infty e^{-\lambda\tau} g_\tau(\tau) d\tau = \frac{a^m}{(a+\lambda)^m}.$$

Equation (22) may then be expressed as

$$\lambda + \alpha - \beta e^{-\lambda\tau_m} \frac{a^m}{(a+\lambda)^m} = 0. \quad (24)$$

Linear systems lose stability when the roots of the characteristic equation cross the imaginary axis from left to right. To study the Hopf bifurcation, we take $\lambda = i\omega$ and $\tan\theta = \frac{\omega}{a}$ to get

$$i\omega + \alpha - \beta(\cos\omega\tau_m - i\sin\omega\tau_m)\frac{a^m}{(a+i\omega)^m} = 0, \quad (25)$$

$$i\omega + \alpha - \beta(\cos\omega\tau_m - i\sin\omega\tau_m)\frac{1}{(1+i\tan\theta)^m} = 0, \quad (26)$$

$$(i\omega + \alpha)(1 + i\tan\theta)^m - \beta(\cos\omega\tau_m - i\sin\omega\tau_m) = 0. \quad (27)$$

Applying de Moivre's theorem [58] and splitting the real and imaginary parts we obtain

$$\alpha(\omega) = \omega\tan(m\theta) + \beta\frac{\cos(\theta)^m}{\cos(m\theta)}\cos\omega\tau_m, \quad (28)$$

$$\beta(\omega) = \frac{\omega + \alpha\tan m\theta}{\frac{\cos(\theta)^m}{\cos(m\theta)}\sin\omega\tau_m}. \quad (29)$$

Finally, coupling the above two equations we may describe the stability contour as a function of egocentric influence α and neighbor influence β as

$$\alpha(\omega) = -\frac{\omega}{\tan(\omega\tau_m - m\tan^{-1}(\omega/a))}, \quad (30)$$

$$\beta(\omega) = -\frac{\omega}{\cos^m(\tan^{-1}(\omega/a))\sin(\omega\tau_m + m\tan^{-1}\frac{\omega}{a})}. \quad (31)$$

Equations (30) and (31) allow one to map the stability transition contour for a given distribution (e.g., specified E and τ_m parameters), as a function of egocentric weight α and neighbour influence weight β curves as a function of frequency ω.

5 Result and Discussion

We analysed 425 trajectories, segmented into 175 solitary insect trajectories (average length of 3 seconds) and 250 group behavior trajectories (average length of 2.5 seconds).

As seen in Table 1, a similar percentage of solo and group trajectories met length requirements for frequency domain identification (55% vs 52%), while the remainder (45% and 48% of trials) were completed in time domain. Average fit percentages were above 80% with standard deviations from 8-16%.

Table 1: Overall Fit Statistics.

Role	Frequency domain			Time domain		
	Trials	Avg.	Std.	Trials	Avg.	Std.
Solo	105	84%	8%	70	81%	16%
Group	112	80%	11%	138	81%	8%

Before discussing overall properties of the identified models, examples of individual identifications in each category are shown.

5.1 Solitary dynamics identification

5.1.1 Example: Frequency domain

105 solo insect frequency domain identifications were conducted. A representative example is shown in camera and 3D views in Figs. 4(b–d) and in the supplementary S1 Video. 3D position coordinates shown in Fig. 4c illustrate the x coordinate tracking behavior.

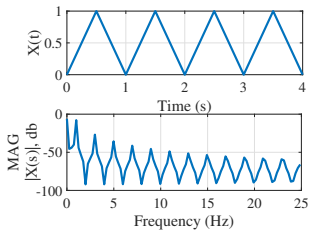

(a) Triangular movement stimulus

(b) Camera-1 view

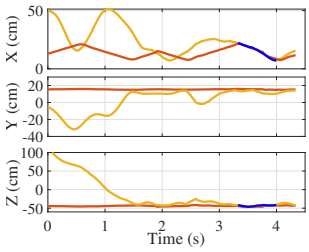

(c) X,Y,Z coordinates

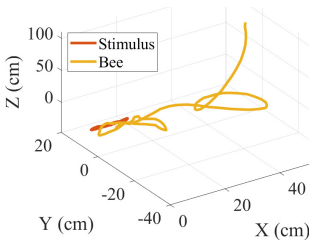

(d) 3D reconstructed trajectories

Fig. 4: (a): A triangular signal was used to apply horizontal entrance movement along the X axis of the world frame, resulting in rich frequency components; (b): a solitary insect's trajectory (length 4 sec) entering the moving entrance is captured by camera-1; (c) & (d): reconstructed position coordinates and 3D trajectory for both input stimulus and insect (blue color indicates Kalman filter).

Frequency transformed stimulus and output signals S_1 and S_2 (respectively) are used to construct a frequency response function, shown in magnitude and phase components for both FFT and CZT transforms in Fig. 5a. A coherent region of response below 1.8Hz is visible, indicating that the input and output have a strong linear relationship (as quantified by $\gamma^2 > 0.6$) in this range. Some deviation from ideal tracking (0dB magnitude, 0° phase) is visible in Fig. 5a, with gain showing some overshoot and a negative phase (lag) indicating a reaction time that quantifies the combined effect of airframe dynamic response due to physics and visuomotor delay. The CZT transform was used to improve resolution in the strongly coherent range (Fig. 5b) below 1.15Hz and the CZT-derived frequency response function $G_{CZT}(s)$ used to identify the equivalent transfer function.

The fit error statistics in Table. 2 indicate a 3 pole, 2 zero transfer function with 15 ms processing latency (transport delay) is the best fit for this example trajectory. The identified model is

Table 2: **Model candidates and performance for an example insect.**

Model Struct.	Fit	FPE	MSE	Delay
2 pole, 1 zero	33.47%	7.77×10^{-3}	7.09×10^{-3}	50ms
3 pole, 3 zero	95.06%	4.56×10^{-5}	3.90×10^{-5}	15ms
4 pole, 3 zero	42.21%	6.44×10^{-3}	5.31×10^{-3}	2ms

$$G_e(s) = e^{-.015s}\frac{0.7377s^2 + 0.5991s^2 + 1.175s + 0.2213}{s^3 + 0.544s^2 + 1.85s + 0.2594}, \tag{32}$$

and a comparison of this identified model and experimental response functions in Fig. 5c show the strong agreement indicated by Table 2. Measured and frequency domain modeled outputs $S_2(\omega)$ show good agreement in Fig. 5c.

Example: Time domain identification

For short trajectories ($\leq$ 1.5 sec), time domain system identification was performed. Fig. 6 shows an example time domain system identification that identified a model

$$G_e(s) = e^{-.04s}\frac{-5.462s + 39.42}{s^2 + 4.471s + 75.86} \tag{33}$$

with a fit percentage of 88.13% and FPE of 1.12×10^{-3}.

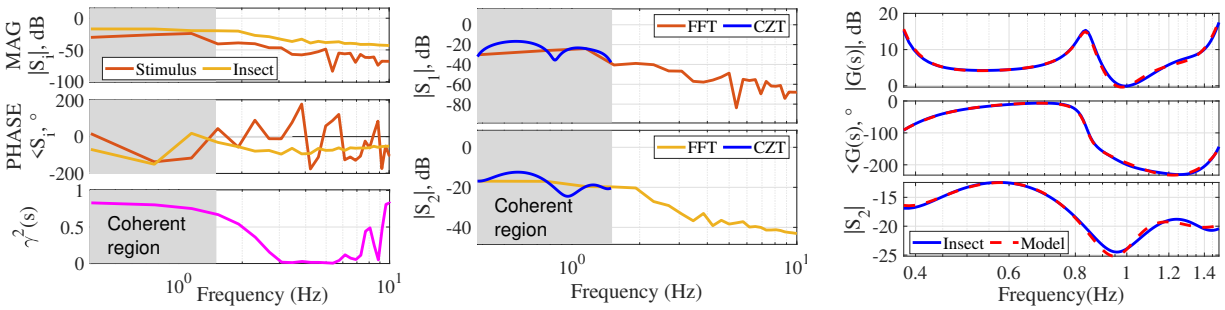

(a) Stimulus and insect data (b) Transform comparison (c) Identified transfer function and model output comparison

Fig. 5: Frequency domain system identification example. (a): Magnitude, phase, and coherence γ^2 plots of the input stimulus S_1 and output (insect) position S_2. A linear relationship between stimulus and insect position is indicated in the shaded region below 1.5 Hz where $\gamma^2 > 0.6$, (b) Comparison of Fourier and Chirp Z-transform magnitudes for stimulus S_1 and insect S_2 in the region of highest coherence, (c): The identified transfer function $G_e(s)$ (dashed red) shows strong agreement with the measured frequency response $G(s)$ (blue) in both magnitude and phase, as do true and identified model output $|S_2|$.

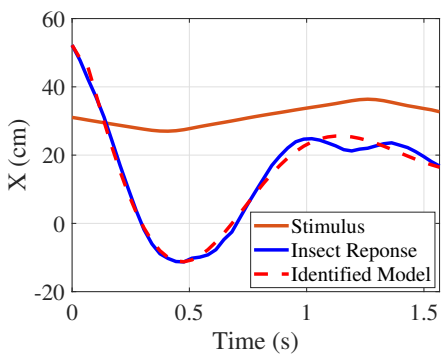

Fig. 6: Example of time domain identifications used for trials $\leq$ 1.5 sec show tracking performance.

5.2 Group dynamics identification

We also identified individual insect dynamics during group approaches to the entrance using the same frequency and time domain identification process. An example of group behavior is shown in Figs. 7(a–b) and in the S2 Video. In this example, insect-1 and insect-2 are identified as a group due to their high coherence ($\gamma > 0.7$ up to 5 Hz). The same frequency and time domain identification tools as in Section 5.1 were applied to extract a dynamic model and corresponding time delay.

5.3 Full dataset and delay distributions

When the identification process was applied to the full dataset of 425 trials, some diversity in identified model structure was seen, as in shown in Fig. 8a. As with the solitary insect example (Table 2), the identification proved insensitive to fit criteria choice (ie, $\mathsf{max}(\mathrm{FIT}), \mathsf{min}(\mathrm{MSE}), \mathsf{min}(\mathrm{FPE})$) across insects measured in this study.

The relative frequency of the identified delays shown in Figs. 8(b–c) show the discovery of two clear effects. First, insect's visuomotor tracking delays are heterogeneous, varying from 7ms to 120ms. Second, insects operating in group settings show a different distribution of delays than those in solitary environments, in particular a significantly narrower distribution. The solitary delay distribution shows a mean of 30ms and standard deviation of 50 ms, while the group delay distribution has an 18ms mean with a significantly narrower 8ms standard deviation.

5.4 Analysis and Simulation

Analysis

To understand the effect of these changing delay distributions in a swarm context, it is helpful to describe the measured distributions functionally. We used a gamma distribution representation with shape parameters of $m = 3.5$, $a = 12$, $\tau_m = 1.85$

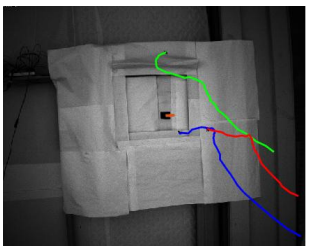

(a) Camera-1 view

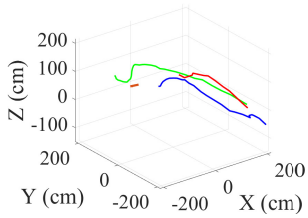

(b) Measured trajectories

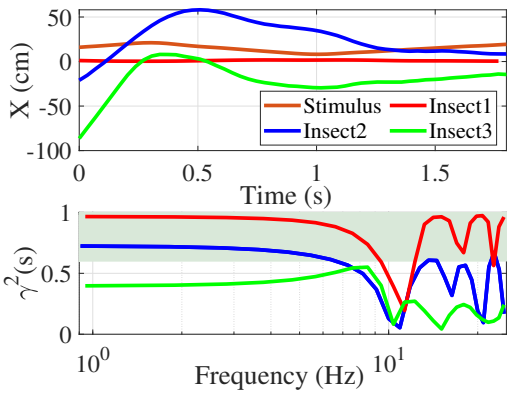

(c) Coherence identifies group insects (#1 and 2).

Fig. 7: Segmentation of group insects by coherence. (a) Three insect flight trajectories in entrance approach as seen by camera-1, (b) Reconstructed 3D flight paths and stimulus, (c) Insect flight trajectories and coherence. Insect1 and Insect2 are identified as group insects due to coherence $\gamma^2 > 0.7$ (shaded area). Insect3's coherence below 0.6 indicates it is not participating in group tracking.

ms in the solo case and $m = 4$, $a = 5$, $\tau_m = 4.1$ ms in the group case, as illustrated in Fig. 8. We used these distribution parameters to find the regions of stability of the swarm model via the parametric equations Eqns. (30) and (31).

The stability regions in Fig. 9 show that for low values of both egocentric and neighbor influence α and β, the swarm remains stable regardless of delay distribution, and high values of neighbor attraction are similarly destabilizing. However, the boundary of swarm stability when using the group delays (red curve) shows a higher tolerance for neighbor attraction than the solitary delay distribution (blue curve). This finding suggests that one function of the delay distribution adjustment seen in group interacting insects is to support cohesion by improving the margin of destabilization.

ω indicates the swarm center's oscillation frequency at the stability boundary, and shows that the delay adjustment also affects the oscillation frequency. In both cases, oscillation frequency on the stability boundary increases with egocentric influence. Group delays show higher oscillation frequencies, indicating that group delays support a higher frequency motion before destabilizing. In many of the recorded experiments, individual trajectory oscillations were observable; current work quantifying the trajectories indicate they are below the limit frequencies in Fig. 9, again suggesting the insects remain below the stability boundary.

Simulation

Some approximation is provided by the swarm model and the curve fit to a gamma distribution, and while the theoretical analysis can assess barycenter stability, it cannot yet predict formation. To explore the validity of the swarm model and examine the effects of the experimental delays, we simulated an interconnected visual swarm with both experimentally-quantified delays and those drawn from the gamma distribution fits, each of which began from randomly distributed initial positions in Fig. 10a.

Simulations using the heterogeneous delays measured in both solo and group delays (ie, the measurements in Fig.8) are shown in Fig. 10 for 100 agents. For theoretical delays the solo swarm used the gamma distribution fit parameters as $\alpha = 7$, $\beta = 6$ and $\frac{m}{a} = .3$, while group used the same α, β and $\frac{m}{a} = 0.78$. The repulsive potential's amplitude and applied distance were taken as $B_r = 0.5$ and $D_r = 1$. The time history of swarm center position in Fig. 10d shows that the swarm center stability failure seen in theoretical analysis persists in the case of experimental delays. Additionally, the simulations show that the instability extends to formation, with group-measured delays stabilizing to a formation in Fig. 10c and solo-measured delays leading to a motion with no observable formation in Fig. 10b.

6 Conclusion

In this study, insects were recorded while tracking a moving visual stimulus in solo and group

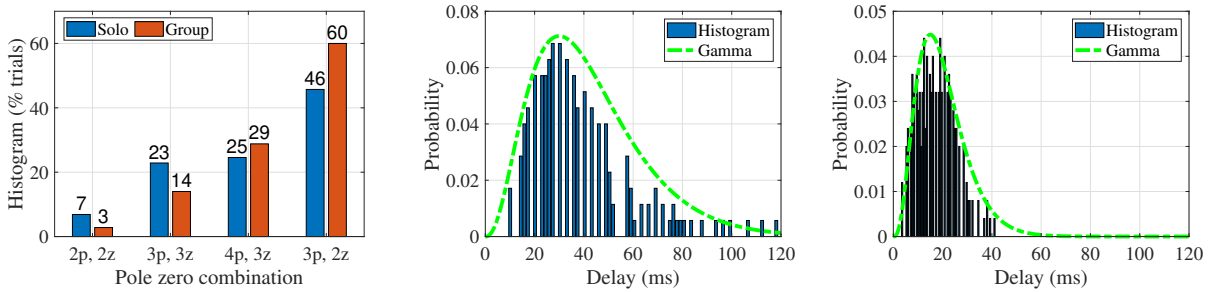

(a) Pole zero combination (b) Delay distribution of solo bees (c) Delay distribution of group bees

Fig. 8: (a). Distribution of identified model structures, as indicated by number of poles and zeros, (b) histogram of solo insect delays vary from 0 to 120 ms and normalized gamma distribution, (c) histogram and fitted distribution curve in group bees, containing a narrower band of delays from 0 to 45 ms.

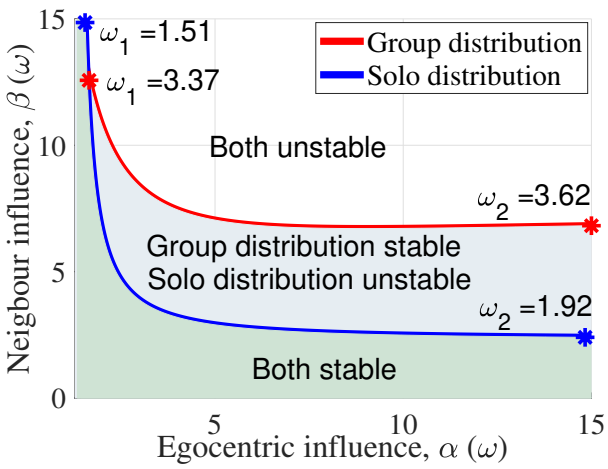

Fig. 9: Stable and unstable regions for the two delay distributions (solo and group) were discovered by applying Eqns.(30) and (31) describing the stability boundary in terms of an individual agent's ego influence α and neighbor influence β. Low neighbor influence factors lead to stable swarm center positions (green region) for either case. As neighbor influence grows, the swarm using a solo distribution loses stability (blue region) before the swarm using group behavior delays loses stability (white region), indicating that the group distribution provides a larger range of response weights (gains) that lead to a stable swarm. As the egocentric weight α grows on the stability boundary, the transition oscillation frequency ω rises.

behaviors and the visuomotor delay in their closed loop tracking was measured. We used a real-time camera-based tracking system that quantified both moving target and insect position in three dimensions. System identification tools were applied to identify the closed loop tracking dynamics between stimulus motion and insect body motion, separating the effects of open loop plant (locomotion) physics from visuomotor feedback delay and quantify the visuomotor delay as a transport delay. The measured insect sensorimotor delays were used to find a delay distribution across population, showing that insect visual sensorimotor feedback delays in a tracking task are heterogeneous across population. Significantly more variation (50ms standard deviation) was found when an insect was the only animal tracking the target, relative to group behaviors in which multiple insects tracked the target (8ms standard deviation). To understand the implications of the measured delays on visually-guided swarms, we then integrated the measured delays into a visually interacting swarm model. Analysis on this model indicates conditions needed for the center of mass's position and allows us to map the stable and unstable regions as a function of behavior. Simulations were conducted using theoretical fits to the delays (gamma distribution) and the experimental delays. The analysis and simulation indicate that the processing delays measured in solitary conditions show unstable swarm behavior and that the group delays provide stable center of mass and cluster shape, and predict the speed of swarm center oscillations at transition.

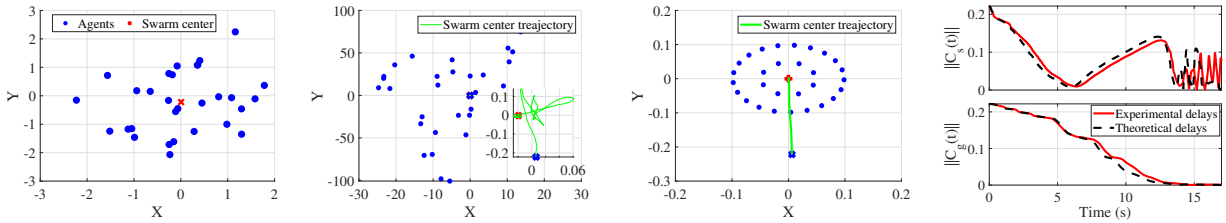

(a) Initial positions, t=0 (b) Solo delays, t=17sec (c) Group delays, t=17sec (d) Swarm center norm

Fig. 10: Swarm simulations with experimental delays for solo and group behaviors. (a) Random initial positions of 30 agents, (b) ending position of agents using experimental solo delays, (c) ending position of agents using experimental group delays (d) time histories of swarm center $C_s(t)$ and $C_g(t)$ norms for solo and group delays, respectively.

Overall, this study quantifies response delays in solo and group tasks and connects these measurements to theoretical limits on the allowable delays for insects in visually guided swarms. The results suggest that insects operating in group contexts adjust their delays to support swarm cohesion. This consistency between experimental measurements of solo and group tasks in flying insects with theoretical and simulated frameworks quantifying constraints is an important outcome for understanding how flying insects support swarming motions despite tight constraints on sensing and feedback. The results provide a foundation for swarming aerial robotics with limited computational resources. For these systems, in which processing delays are significant, knowledge of what delay distributions support stable motions will guide engineers in distributing processing tasks appropriately.

Supporting information

S1 Video.

Solo behavior. Solitary insects track the entrance in this video.

S2 Video.

Group behavior. A subset of the 10 insects in this video track the moving entrance.

Acknowledgments

This work was supported in part by ONR Young Investigator Award N00014-19-1-2216.

Data availability statement

The data used in this experiment is available at <*link added on publication*>.

Authorship contributions:

SI: Conceptualization, Methodology, Investigation, Software, Writing- Original draft preparation, Visualization, Writing- Reviewing and Editing. IAF: Supervision, Project administration, Funding acquisition, Conceptualization, Investigation, Writing- Original draft preparation, Visualization, Writing- Reviewing and Editing

Competing interests

The authors declare no competing interests.

References

[1] Schranz, M. *et al.* Swarm intelligence and cyber-physical systems: concepts, challenges and future trends. *Swarm and Evolutionary Computation* **60**, 100762 (2021) .

[2] Campion, M., Ranganathan, P. & Faruque, S. Uav swarm communication and control architectures: a review. *Journal of Unmanned Vehicle Systems* **7** (2), 93–106 (2018) .

[3] Jaffe, J. S. *et al.* A swarm of autonomous miniature underwater robot drifters for exploring submesoscale ocean dynamics. *Nature Communications* **8** (1), 14189 (2017).

URL https://doi.org/10.1038/ncomms14189. https://doi.org/10.1038/ncomms14189 .

[4] Billah, M. A. & Faruque, I. A. Bioinspired visuomotor feedback in a multiagent group/swarm context. *IEEE Transactions on Robotics* **37** (2), 603–614 (2020) .

[5] Taylor, G. K. & Krapp, H. G. Sensory systems and flight stability: what do insects measure and why? *Advances in insect physiology* **34**, 231–316 (2007) .

[6] Jeschke, J. M. & Tollrian, R. Prey swarming: which predators become confused and why? *Animal Behaviour* **74** (3), 387–393 (2007) .

[7] Islam, M. S. & Faruque, I. A. Experimental identification of individual insect visual tracking delays in free flight and their effects on visual swarm patterns. *bioRxiv* (2022). https://doi.org/10.1101/2022.04.06.487367 .

[8] Parrish, J. K. & Edelstein-Keshet, L. Complexity, pattern, and evolutionary trade-offs in animal aggregation. *Science* **284** (5411), 99–101 (1999). https://doi.org/10.1126/science.284.5411.99 .

[9] Berdahl, A., Torney, C. J., Ioannou, C. C., Faria, J. J. & Couzin, I. D. Emergent sensing of complex environments by mobile animal groups. *Science* **339** (6119), 574–576 (2013). https://doi.org/10.1126/science.1225883 .

[10] Krause, J., Ruxton, G. D. & Krause, S. Swarm intelligence in animals and humans. *Trends in Ecology & Evolution* **25** (1), 28–34 (2010). URL https://www.sciencedirect.com/science/article/pii/S0169534709002298. https://doi.org/https://doi.org/10.1016/j.tree.2009.06.016 .

[11] Swain, D. T., Couzin, I. D. & Ehrich Leonard, N. Real-time feedback-controlled robotic fish for behavioral experiments with fish schools. *Proceedings of the IEEE* **100** (1), 150–163 (2012). https://doi.org/10.1109/JPROC.2011.2165449 .

[12] Ni, R. & Ouellette, N. T. On the tensile strength of insect swarms. *Physical Biology* **13** (4), 045002 (2016). https://doi.org/10.1088/1478-3975/13/4/045002 .

[13] Tennenbaum, M., Liu, Z., Hu, D. & Fernandez-Nieves, A. Mechanics of fire ant aggregations. *Nature Materials* **15** (1), 54–59 (2016). URL https://doi.org/10.1038/nmat4450. https://doi.org/10.1038/nmat4450 .

[14] Baird, E., Srinivasan, M. V., Zhang, S. & Cowling, A. Visual control of flight speed in honeybees. *Journal of Experimental Biology* **208** (20), 3895–3905 (2005). https://doi.org/10.1242/jeb.01818 .

[15] Fry, S. N., Rohrseitz, N., Straw, A. D. & Dickinson, M. H. Visual control of flight speed in Drosophila melanogaster. *Journal of Experimental Biology* **212** (8), 1120–1130 (2009). https://doi.org/10.1242/jeb.020768 .

[16] Farina, W. M., Varjú, D. & Zhou, Y. The regulation of distance to dummy flowers during hovering flight in the hawk moth macroglossum stellatarum. *Journal of Comparative Physiology A* **174**, 239–247 (2004) .

[17] Straw, A. D., Branson, K., Neumann, T. R. & Dickinson, M. H. Multi-camera realtime 3d tracking of multiple flying animals (2010). 1001.4297.

[18] Noldus, L. P., Spink, A. J. & Tegelenbosch, R. A. EthoVision: a versatile video tracking system for automation of behavioral experiments. *Behav Res Methods Instrum Comput* **33** (3), 398–414 (2001) .

[19] Fry, S. *et al.* Context-dependent stimulus presentation to freely moving animals in 3d. *Journal of Neuroscience Methods* **135** (1), 149–157 (2004). https://doi.org/https://doi.org/10.1016/j.jneumeth.2003.12.012 .

[20] Pérez-Escudero, A., Vicente-Page, J., Hinz, R. C., Arganda, S. & de Polavieja, G. G. idtracker: tracking individuals in a group by automatic identification of unmarked animals. *Nature Methods* **11** (7), 743–748 (2014) .

[21] Rodriguez, A. *et al.* Toxtrac: A fast and robust software for tracking organisms. *Methods in Ecology and Evolution* **9** (3), 460–464 (2018). https://doi.org/https://doi.org/10.1111/2041-210X.12874 .

[22] van der Vaart, K., Sinhuber, M., Reynolds, A. M. & Ouellette, N. T. Mechanical spectroscopy of insect swarms. *Science Advances* **5** (7), eaaw9305 (2019). https://doi.org/10.1126/sciadv.aaw9305 .

[23] Downe, A. E. R. & Caspary, V. G. The swarming behaviour of chironomus riparius (diptera: Chironomidae) in the laboratory. *The Canadian Entomologist* **105** (1), 165–171 (1973). https://doi.org/10.4039/Ent105165-1 .

[24] Puckett, J. G. & Ouellette, N. T. Determining asymptotically large population sizes in insect swarms. *Journal of The Royal Society Interface* **11** (99), 20140710 (2014). URL https://royalsocietypublishing.org/doi/abs/10.1098/rsif.2014.0710. https://doi.org/10.1098/rsif.2014.0710 .

[25] Sprayberry, J. D. H. & Daniel, T. L. Flower tracking in hawkmoths: behavior and energetics. *Journal of Experimental Biology* **210** (1), 37–45 (2007). https://doi.org/10.1242/jeb.02616 .

[26] Matthews, M. & Sponberg, S. Hawkmoth flight in the unsteady wakes of flowers. *Journal of Experimental Biology* **221** (22) (2018). https://doi.org/10.1242/jeb.179259 .

[27] Sponberg, S., Dyhr, J. P., Hall, R. W. & Daniel, T. L. Luminance-dependent visual processing enables moth flight in low light. *Science* **348** (6240), 1245–1248 (2015). https://doi.org/10.1126/science.aaa3042 .

[28] Stöckl, A. L., Kihlström, K., Chandler, S. & Sponberg, S. Comparative system identification of flower tracking performance in three hawkmoth species reveals adaptations for dim light vision. *Philos Trans R Soc Lond B Biol Sci* **372** (1717) (2017) .

[29] Jain, P., Singh, O. P. & Butail, S. Dynamics of mosquito swarms over a moving marker (2020). 2007.04254.

[30] Lewis, J. Autoinhibition with transcriptional delay: A simple mechanism for the zebrafish somitogenesis oscillator. *Current Biology* **13** (16), 1398–1408 (2003). https://doi.org/https://doi.org/10.1016/S0960-9822(03)00534-7 .

[31] Morelli, L. G. *et al.* Delayed coupling theory of vertebrate segmentation. *HFSP journal* **3** (1), 55–66 (2009). URL https://doi.org/10.2976/1.3027088 .

[32] MacDonald, N. Biological delay systems: Linear stability theory. *Acta Applicandae Mathematica* **18** (3), 297–300 (1990). https://doi.org/10.1007/BF00049132 .

[33] Okubo, A. Dynamical aspects of animal grouping: swarms, schools, flocks, and herds. *Advances in biophysics* **22**, 1–94 (1986) .

[34] Reynolds, C. W. Flocks, herds and schools: A distributed behavioral model. *ACM SIGGRAPH Computer Graphics* 25–34 (1987) .

[35] Ling, H. *et al.* Costs and benefits of social relationships in the collective motion of bird flocks. *Nature ecology & evolution* **3** (6), 943–948 (2019) .

[36] Bellomo, N. & Brezzi, F. Challenges in active particles methods: Theory and applications. *Mathematical Models and Methods in Applied Sciences* **28** (09), 1627–1633 (2018). https://doi.org/10.1142/S0218202518020013 .

[37] Vicsek, T., Czirók, A., Ben-Jacob, E., Cohen, I. & Shochet, O. Novel type of phase transition in a system of self-driven particles. *Phys. Rev. Lett.* **75**, 1226–1229 (1995). https://doi.org/10.1103/PhysRevLett.75.1226 .

[38] Bellomo, N. & Brezzi, F. Challenges in active particles methods: Theory and applications. *Mathematical Models and Methods in Applied Sciences* **28** (09), 1627–1633 (2018). URL https://doi.org/10.

1142/S0218202518020013. https://doi.org/10.1142/S0218202518020013 .

[39] Rossi, F., Bandyopadhyay, S., Wolf, M. & Pavone, M. Review of multi-agent algorithms for collective behavior: a structural taxonomy. *IFAC-PapersOnLine* **51** (12), 112–117 (2018) .

[40] Rimon, E. & Koditschek, D. Exact robot navigation using artificial potential functions. *IEEE Transactions on Robotics and Automation* **8** (5), 501–518 (1992). https://doi.org/10.1109/70.163777 .

[41] Gazi, V. On lagrangian dynamics based modeling of swarm behavior. *Physica D Nonlinear Phenomena* **260**, 159–175 (2013). https://doi.org/10.1016/j.physd.2013.06.010 .

[42] Liao, X., Wu, Z. & Yu, J. Stability switches and bifurcation analysis of a neural network with continuously delay. *IEEE Transactions on Systems, Man, and Cybernetics - Part A: Systems and Humans* **29** (6), 692–696 (1999). https://doi.org/10.1109/3468.798076 .

[43] Guo, S. & Li, J. Bifurcation theory of functional differential equations: a survey. *Journal of Applied Analysis and Computation* **5**, 751–766 (2015) .

[44] Bennet, D. J. & McInnes, C. R. Distributed control of multi-robot systems using bifurcating potential fields. *Robotics and Autonomous Systems* **58** (3), 256–264 (2010). https://doi.org/https://doi.org/10.1016/j.robot.2009.08.004, towards Autonomous Robotic Systems 2009: Intelligent, Autonomous Robotics in the UK .

[45] Kolpas, A. *et al.* How the spatial position of individuals affects their influence on swarms: a numerical comparison of two popular swarm dynamics models. *PloS one* **8** (3), e58525 (2013) .

[46] Sinhuber, M., Vaart, K., Feng, Y., Reynolds, A. & Ouellette, N. An equation of state for insect swarms. *Scientific Reports* **11** (2021). https://doi.org/10.1038/s41598-021-83303-z .

[47] Cucker, F. & Smale, S. Emergent behavior in flocks. *IEEE Transactions on Automatic Control* **52** (5), 852–862 (2007). https://doi.org/10.1109/TAC.2007.895842 .

[48] Roussel, M. R. The use of delay differential equations in chemical kinetics. *The Journal of Physical Chemistry* **100** (20), 8323–8330 (1996). https://doi.org/10.1021/jp9600672 .

[49] MacDonald, N. Time lag in a model of a biochemical reaction sequence with end product inhibition. *Journal of Theoretical Biology* **67** (3), 549–556 (1977). https://doi.org/https://doi.org/10.1016/0022-5193(77)90056-X .

[50] Morelli, L. & Jülicher, F. Precision of genetic oscillators and clocks. *Physical review letters* **98**, 228101 (2007). https://doi.org/10.1103/PhysRevLett.98.228101 .

[51] Feng, J., Sevier, S. A., Huang, B., Jia, D. & Levine, H. Modeling delayed processes in biological systems. *Phys. Rev. E* **94**, 032408 (2016). https://doi.org/10.1103/PhysRevE.94.032408 .

[52] Glass, D. S., Jin, X. & Riedel-Kruse, I. H. Nonlinear delay differential equations and their application to modeling biological network motifs. *Nature Communications* **12** (1), 1788 (2021). URL https://doi.org/10.1038/s41467-021-21700-8 .

[53] Himakalasa, A. & Wongkaew, S. Stability analysis of swarming model with time delays. *Advances in Difference Equations* **2021** (1), 217 (2021). https://doi.org/10.1186/s13662-021-03379-9 .

[54] Lindley, B., Mier-Y-Teran-Romero, L. & Schwartz, I. B. Randomly distributed delayed communication and coherent swarm patterns. *IEEE Int Conf Robot Autom* (2012) .

[55] Szwaykowska, K., Romero, L. M.-y.-T. & Schwartz, I. B. Collective motions of heterogeneous swarms. *IEEE Transactions on Automation Science and Engineering* **12** (3),

810–818 (2015). https://doi.org/10.1109/TASE.2015.2403253 .

[56] Svoboda, T., Martinec, D. & Pajdla, T. A convenient multicamera self-calibration for virtual environments. *Presence* **14** (4), 407–422 (2005). https://doi.org/10.1162/105474605774785325 .

[57] Ljung, L. *System Identification: Theory for the User* Prentice Hall information and system sciences series (Prentice Hall PTR, 1999). URL https://books.google.com/books?id=nHFoQgAACAAJ.

[58] Bernard, S., Bélair, J. & Mackey, M. Sufficient conditions for stability of linear differential equations with distributed delay. *Discrete and Continuous Dynamical Systems. Series B* **1** (2001). https://doi.org/10.3934/dcdsb.2001.1.233 .

Appendix: Written Supplementary Information

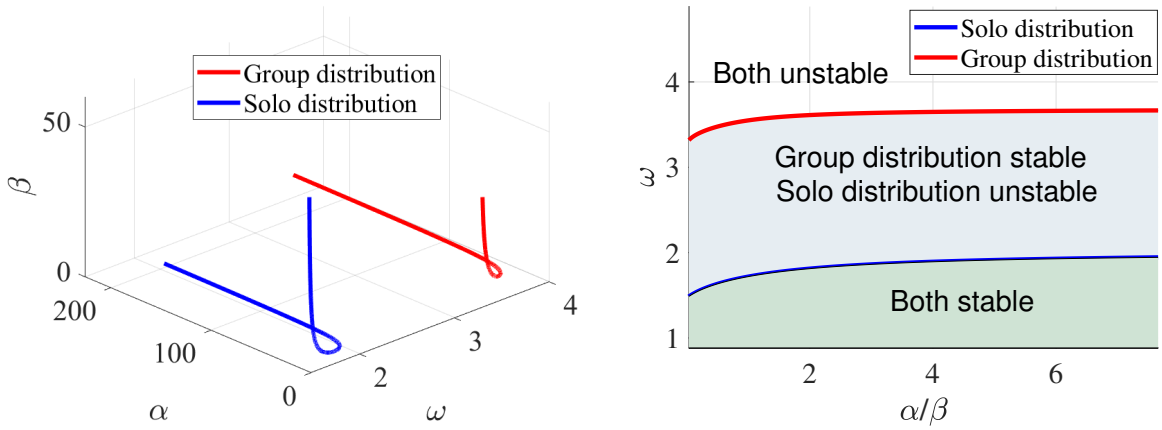

(a) 3D plot showing α, β as a function of changing ω

(b) Ratio of two weights

Fig. 11: Additional views of stability plots